Nonreciprocal transport of superconductivity in a Bi/Ni bilayer

Ranran Cai,[1,*,†,‡] Di Yue,[2,*] Weiliang Qiao,[1] Liangliang Guo,[1] Zidan Chen,[1] X. C. Xie,[1,3,4] Xiaofeng Jin,[2] and Wei Han[1,§]

[1]*International Center for Quantum Materials, School of Physics, Peking University, Beijing 100871, People's Republic of China*

[2]*State Key Laboratory of Surface Physics and Department of Physics, Fudan University, Shanghai 200433, People's Republic of China*

[3]*Institute for Nanoelectronic Devices and Quantum Computing, Fudan University, Shanghai 200433, People's Republic of China*

[4]*Hefei National Laboratory, Hefei 230088, People's Republic of China*

(Received 20 May 2023; accepted 19 July 2023; published 4 August 2023)

Nonreciprocal transport, an exciting quantum physical phenomenon arising from symmetry breaking, can be significantly magnified in the superconducting state. Recent progresses have demonstrated it as a unique probe of the pairing mechanisms in symmetry-breaking superconductors (SCs). Here, we report the nonreciprocal charge transport of the superconductivity in the Bi/Ni bilayer, a *p*-wave SC candidate. The nonreciprocal transport signal is dramatically enhanced under in-plane magnetic field, but vanishes under perpendicular magnetic field. Interestingly, the nonreciprocal transport is magnified in the temperature regime that can be associated with notable vortex motion. Our results provide compelling evidence for the Rashba superconductivity in the Bi/Ni bilayer with in-plane spin splitting, a precursor for the *p*-wave SC, which might hold promise for future topological quantum computing applications.

DOI: 10.1103/PhysRevB.108.064501

I. INTRODUCTION

The *p*-wave superconductor (SC), a long-sought novel quantum state [1–3], has attracted a lot of attention due to its interesting physical properties and potential technological impact for fault-tolerant topological quantum computing [4,5]. The superconducting Bi/Ni bilayer has been shown to be a promising chiral *p*-wave SC candidate [6], arising from the time and spatial reversal symmetry breaking. The *p*-wave pairing has been evidenced in recent experiments, including point contact Andreev reflection [7], phase sensitive quantum interference [8], and time-domain terahertz spectroscopy [9], etc., while other types of pairing symmetry have also been suggested, such as $d_{xy} \pm id_{x^2+y^2}$ based on Kerr rotation using a Sagnac interferometer [10], and conventional *s*-wave pairing of Bi-Ni alloys formed at the Bi/Ni interface [11,12]. These important progresses show that the pairing symmetry of the superconductivity in the Bi/Ni bilayer is an important question that needs further investigation.

Nonreciprocal transport is a unique physical phenomenon arising from intrinsic symmetry breaking in quantum materials [13–16]. It can be significantly magnified in noncentrosymmetric SCs [17,18] and their heterostructures, including transition metal disulfide [19,20], oxide interfacial two-dimensional electron gases (2DEGs) [21], kagome SC CsV_3Sb_5 [22,23], and SC proximitized heterostructures [24–26]. A special nonreciprocity is the superconducting diode effect, which has been observed in superconducting superlattice [27,28] and Josephson junctions [29,30]. The superconducting diode effect holds the promising potential for low-power superconducting circuits applications [31]. Most importantly, since the nonreciprocal transport is associated with symmetry-breaking induced spin-splitting Fermi surfaces [17], it provides a unique means to explore the pairing symmetry in noncentrosymmetric SCs [19,21,24].

Here, we report the nonreciprocal transport of the superconductivity in the Bi/Ni bilayer with spin-splitting Fermi surface [17,18]. These results further suggest that superconductivity at the Bi/Ni bilayer is a promising *p*-wave SC candidate.

II. EXPERIMENT

The Bi (20 nm)/Ni (3 nm) bilayers were grown on the single-crystalline (001)-oriented MgO substrates in an ultrahigh vacuum molecular beam epitaxy system with base pressure of 6×10^{-8} Pa [7,10]. Prior to the growth, the MgO substrates were cleaned by annealing at 700 °C in vacuum for 75 min. Then the Ni layer and Bi layer were sequentially deposited onto MgO at 300 and 110 °C, respectively. The Hall bar devices of the Bi/Ni bilayers were patterned using standard electron-beam lithography, followed by argon ion-beam etching. The optical image of a typical Bi/Ni Hall bar device is shown in Fig. 1(b). The electrical transport measurements were carried out in a physical properties measurement system (PPMS; Quantum Design) using the AC lock-in technique. During the measurement, an AC current (frequency: $f = 7$ Hz) is applied between the source and drain ($I_{sd} = 100$ μA) using a Keithley 6221, as illustrated in Fig. 1(b). The first and second harmonic voltages ($V^{1\omega}$ and $V^{2\omega}$) were simultaneously measured by two lock-in amplifiers

*These authors contributed equally to the work.

†Present address: CAS Key Laboratory of Quantum Information, University of Science and Technology of China, Hefei, Anhui 230026, P. R. China.

‡Corresponding author: cairanran@ustc.edu.cn

§Corresponding author: weihan@pku.edu.cn

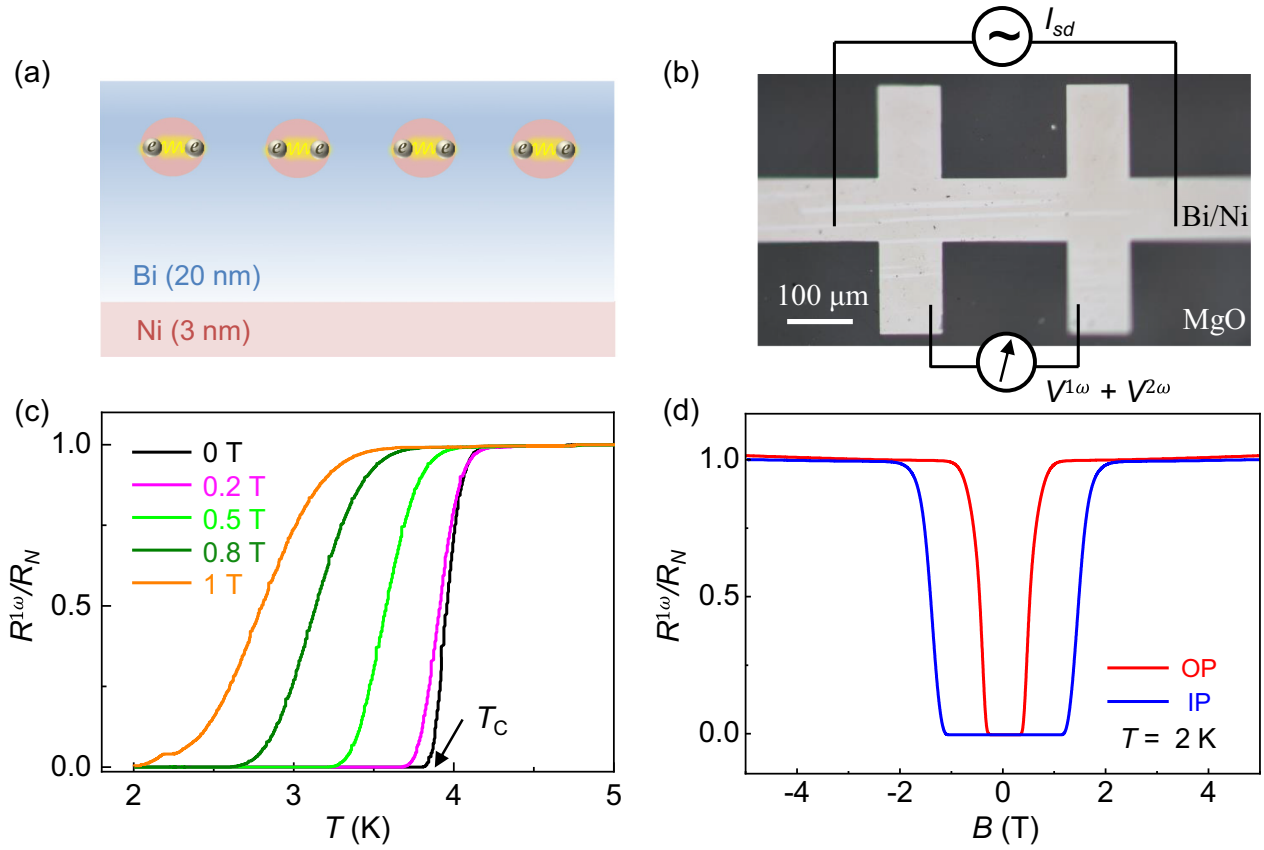

FIG. 1. Basic characterization of the superconductivity in a Bi/Ni bilayer. (a) Schematic of superconductivity in Bi (20 nm)/Ni (3 nm) bilayer. (b) Optical picture of the Hall bar device fabricated on the Bi/Ni bilayer. (c) Temperature dependence of the channel resistance $R^{1\omega}$ of the Hall bar device under various out-of-plane magnetic fields from 0 to 1 T. The $R^{1\omega}$ is normalized by the values at $T = 5$ K. The superconducting transition temperature (T_c) is obtained to be ∼3.8 K, from the zero-resistance state at $B = 0$ T. (d) Out-of-plane (OP, red line) and in-plane (IP, blue line) magnetic field dependencies of normalized channel resistance at $T = 2$ K. The $R^{1\omega}$ is normalized by the normal state resistance at $B = 5$ T.

(SR830) with the probed phases set at 0 and 90 °, respectively. During the measurements of the phase diagram as a function of magnetic field and field direction, the Bi/Ni Hall bar devices were rotated between 0 and 360 ° via a rotation sample holder under a constant magnetic field in the PPMS.

III. RESULTS AND DISCUSSION

The Bi/Ni bilayer consists of a 20-nm-thick Bi layer and a 3-nm-thick Ni layer, which are epitaxially grown on the MgO substrates [7,10]. As shown in Fig. 1(a), the Cooper pairs exist at the Bi top interface away from the Ni layer [7]. Transport measurements are carried out on the Hall bar devices of Bi/Ni bilayers using standard low-frequency lock-in technique, as illustrated in Fig. 1(b). Figure 1(c) shows the normalized resistance ($R^{1\omega}/R_N$, where R_N is the measured resistance at normal state at $T = 5$ K) as a function of the temperature (T) under various out-of-plane magnetic fields (B_{OP}) measured on device A. The superconducting transition temperature (T_c) is determined to be ∼3.8 K from the zero-resistance state. As the magnetic field increases, a superconductor-to-metal transition is observed. Figure 1(d) shows the magnetic field dependence of the channel resistance at $T = 2$ K under B_{OP} and in-plane magnetic field (B_{IP}), respectively. The out-of-plane and in-plane critical magnetic fields are determined to be ∼0.32 and ∼1.15 T, respectively, and the in-plane critical magnetic field at $T = 0$ K is estimated to be ∼1.27 T, as shown in Fig. S1 of the Supplemental Material [32].

The inversion-symmetry breaking of the Bi/Ni bilayer induces the spin-orbit coupling (SOC) at the interface which will break the spin degeneracy of the energy band with spin splitting, as illustrated in Fig. 2(a) for an in-plane spin splitting Fermi surface of Bi(110) [33,34] accompanied by strong spin-momentum lock-in property. The applied B_{IP} first causes the accumulation of spin angular momentum, which is then converted into charge momentum under the action of spin-momentum lock-in to contribute the additional charge current [light green arrow in Fig. 2(a)] named renormalized current I_r. Depending on the magnetic field direction, the I_r can be parallel or antiparallel with the applied charge current I_{sd}. As a result, the charge transport will depend on the current and magnetic field directions; namely the nonreciprocal transport effect [13]. Quantitatively, the nonreciprocal transport effect

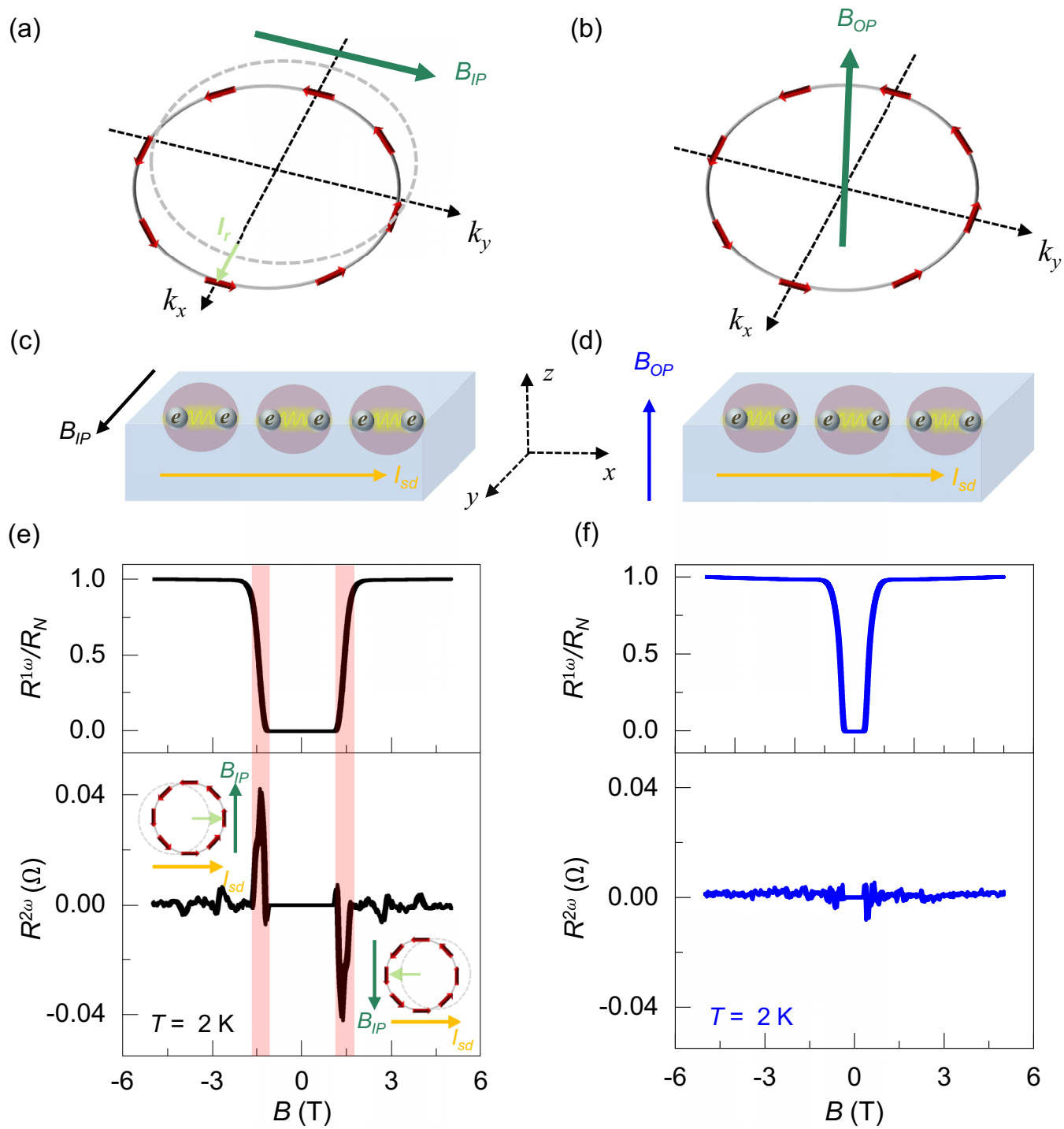

FIG. 2. Nonreciprocal transport of the superconductivity in a Bi/Ni bilayer. (a) Schematic of in-plane magnetic field (B_{IP}) induced Fermi surface shift for an in-plane spin splitting system. (b) Schematic of Fermi surface under an out-of-plane magnetic field (B_{OP}). (c), (d) Schematics of the measurement geometry under B_{IP} and B_{OP}, respectively. (e) The channel resistance ($R^{1\omega}$) and nonreciprocal resistance ($R^{2\omega}$) as a function of B_{IP} at $T = 2$ K. The nonreciprocal transport is highlighted by red shadow region. Insets: Illustration of the physical pictures accounting for nonreciprocal signal $R^{2\omega}$. (f) The channel resistance ($R^{1\omega}$) and nonreciprocal resistance ($R^{2\omega}$) as a function of B_{OP} at $T = 2$ K.

appears in the nonlinear response of IV characteristic as expressed in the following equation:

$$V = R_0 I_{sd} + \gamma R_0 B I_{sd}^2, \quad (1)$$

where B is the magnetic field perpendicular to I_{sd}, R_0 is the ordinary Ohm resistance, and γ is the nonreciprocal transport coefficient. Since the nonlinear term is much smaller than the linear term, making it challenging to detect the nonreciprocal part using DC measurement (Fig. S2 [32]), the AC lock-in

technique is used to measure the nonreciprocal effect. Under the AC current of $I_{sd}\sin\omega t$, Eq. (1) can be further expressed by the equation below [21]:

$$V = V^{1\omega} + V^{2\omega} + \ldots = R_0 I_{sd}\sin\omega t + \frac{1}{2}\gamma R_0 B I_{sd}^2\left\{1 + \sin\left(2\omega t - \frac{\pi}{2}\right)\right\}, \quad (2)$$

where the second term can be easily detected by lock-in amplifier using the second harmonic ($V^{2\omega}$) setting. In these two equations, the first part is the ordinary ohmic law and the second part represents the nonreciprocal transport, indicating that it is proportional to the magnetic field (B) and I_{sd}. The polarity of the second term is determined by the magnetic field direction indicating that the B induced renormalization current (I_r) dominates the nonreciprocal transport via the spin-splitting energy band which is generated by Rashba spin-orbit coupling (SOC) at the Bi/Ni bilayer. To measure the nonreciprocal transport of the superconductivity at the Bi/Ni bilayer, the first ($V^{1\omega}$) and second ($V^{2\omega}$) harmonic voltages are measured with I_{sd} along the x-axis direction and B in the yz plane that is always perpendicular to the I_{sd} direction, as illustrated in Figs. 2(c) and 2(d). The first and second harmonic resistances are obtained as $R^{1\omega} = V^{1\omega}/I_{sd}$ and $R^{2\omega} = V^{2\omega}/I_{sd}$, and the nonreciprocal transport coefficient can be expressed as

$$\gamma = \frac{2R^{2\omega}}{R^{1\omega}BI_{sd}}. \quad (3)$$

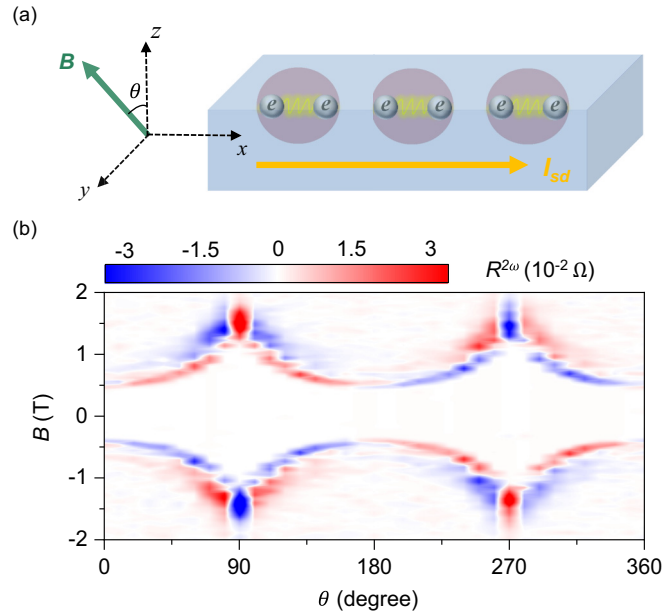

FIG. 3. Magnetic field dependence of the nonreciprocal transport of superconductivity in Bi/Ni bilayer. (a) Schematic of measurement geometry with magnetic field (B) rotating in the yz plane. The current (I_{sd}) is along x axis. θ is magnetic field angle. (b) The phase diagram of $R^{2\omega}$ as a function of B and θ.

Figure 2(e) shows the first and second harmonic resistances as a function of B_{IP} at $T = 2$ K (device A). When the Bi/Ni bilayer undergoes the transition between the normal and superconducting states, $R^{1\omega}/R_N$ suddenly decreases and $R^{2\omega}$ is dramatically enhanced [red shadow region in Fig. 2(e)]. $R^{2\omega}$ reaches the maximum at $B_{IP} \sim 1.2$ T, and decreases when the magnetic field further decreases, which is due to the gradually vanishing of channel resistance for the Bi/Ni bilayer approaching the superconductivity state [19]. The nonreciprocal signal changes its sign as the magnetic field changes its direction. This observation is expected for 2D noncentrosymmetric SCs with in-plane spin-splitting Fermi surfaces [17]. As illustrated in the insets of Fig. 2(e), positive (or negative) B_{IP} induces a Fermi surface shift and generates a renormalized current (I_r) contribution (light green arrows), leading to the positive (or negative) $R^{2\omega}$. On the other hand, the in-plane spin-splitting bands will not be affected by the out-of-plane magnetic field (B_{OP}) as illustrated in Fig. 2(b) which results in the absence of a nonreciprocal transport signal under B_{OP} [Fig. 2(f)]. These results strongly confirm that Bi/Ni superconductivity pairing agrees well with the theoretical prediction of Rashba SC with in-plane spin splitting, which could lead to a spin-triplet p-wave component by reselecting a spin quantum axis [35–38].

To further explore the symmetry of the nonreciprocal transport signal, we perform the $R^{2\omega}$ vs B measurements on another Bi/Ni Hall bar device (device B) with rotating the magnetic field direction in the yz plane and I_{sd} along the x axis, as illustrated in Fig. 3(a). The phase diagram of $R^{2\omega}$ [Fig. 3(b)] shows the 2π symmetry as a function of θ, which is further consistent with the theoretical prediction of the 2D Rashba SC with in-plane spin splitting [17]. As the B slightly deviates from the y axis, $R^{2\omega}$ vs B shows a double peak feature with sign reversal suggesting that other possible competing mechanisms of nonreciprocal transport might exist in the Bi/Ni bilayer, such as the vortex Nernst effect [26] or the competition between different types of vortex [20,25]. Future studies are needed to fully understand this sign reversal feature. Nevertheless, the rotating magnetic-field-induced sign reversal of $R^{2\omega}$ vs B has only recently been observed in our Bi/Ni bilayer, a p-wave SC candidate, and topological insulator/SC heterostructures [25], which was attributed to the competition between the spontaneous vortex in the BKT phase and the out-of-plane B component induced vortex. More importantly, the recently reported extrinsic nonreciprocal mechanisms [39,40], exhibit strong dependence on the out-of-plane magnetic field. However, in our experiment, $R^{2\omega}$ vanishes $\theta = 0$ degree, when the field is in the out-of-plane direction. This feature indicates that the nonreciprocal signal in the Bi/Ni bilayer is most likely to be intrinsic, arising from the in-plane spin-splitting pairing.

To further explore the nonreciprocal mechanisms in the Bi/Ni bilayer, we perform the measurements at various temperatures and B_{IP}, and the results (device A) are summarized in Fig. 4(a). Clearly, the enhanced peak behaviors of $R^{2\omega}$ are observed around the superconductor-to-metal transition regime, consistent with the phase diagram of $R^{1\omega}$ (Fig. S3 [32]). Specifically, the magnetic field dependence of $R^{2\omega}$ at $T = 2.5$, 3, 3.5, and 4 K are extracted as shown in Fig. 4(b). As temperature increases, the amplitude of $R^{2\omega}$ monotonically decreases then eventually disappear at $T = 4$ K. More interestingly, the double-peak feature can be observed at $T = 3.5$ K, which is consistent with the sign reversal patterns in Fig. 4(a) around 3.5 K. This temperature variation induced sign reversal behavior is also similar to previous results

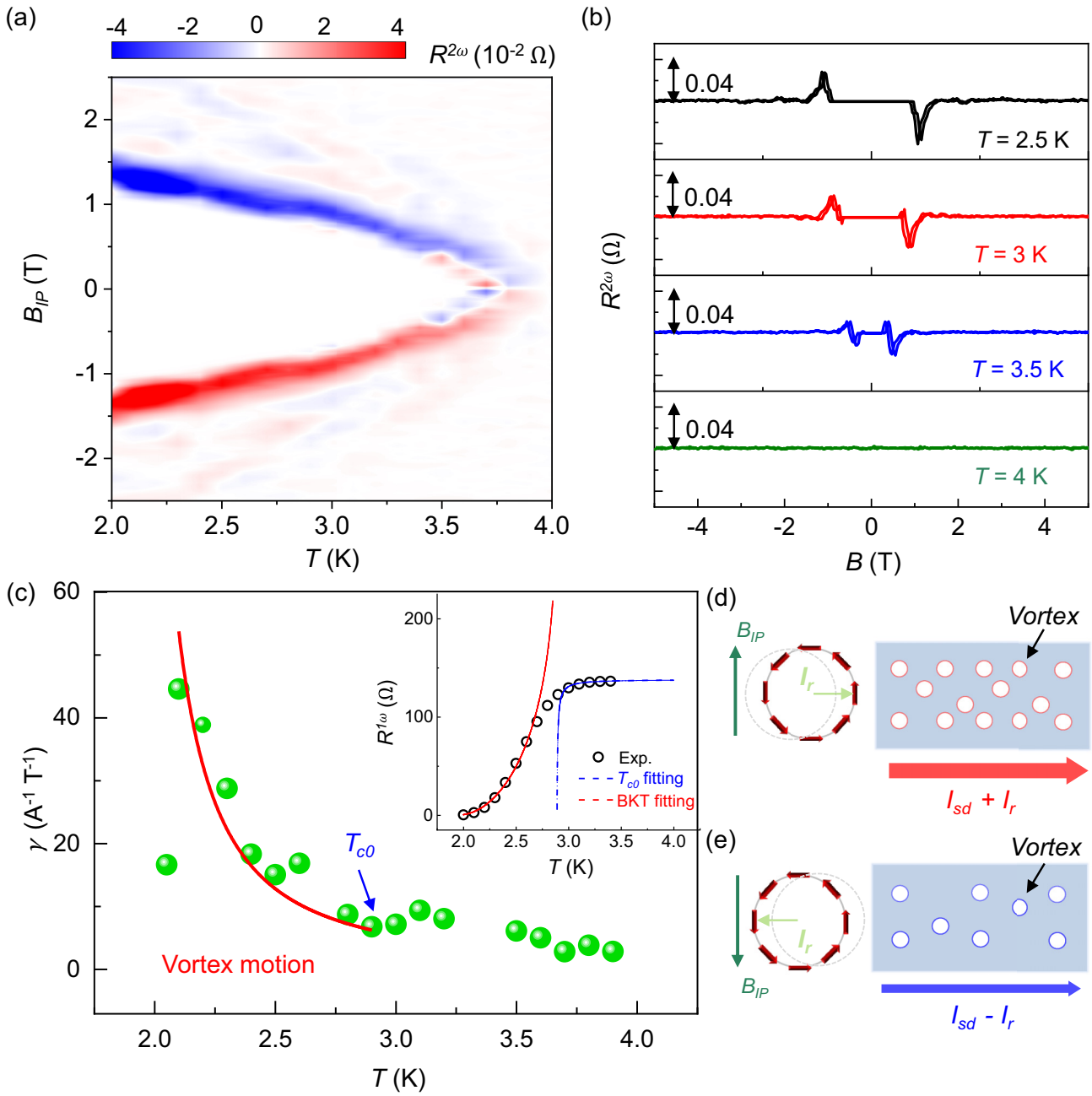

FIG. 4. Temperature dependence of the nonreciprocal transport of superconductivity in Bi/Ni bilayer. (a) Phase diagram of $R^{2\omega}$ as a function of temperature (T) and in-plane magnetic field (B_{IP}). (b) Magnetic field dependence of $R^{2\omega}$ measured at $T = 2.5$, 3, 3.5, and 4 K, respectively. (c) Temperature-dependent nonreciprocal coefficient ($\gamma = \frac{2R^{2\omega}}{R^{1\omega} BI_{sd}}$). The red line represents the best fitting curve for the vortex motion regime based on the equation of $\gamma = c(T - T_{BKT})^{-1.5}$. Inset: The mean field fitting (blue dash line) and the BKT fitting (red dash line) of temperature dependence of $R^{1\omega}$ at $B = 1.2$ T. (d,e) Schematics of higher/lower vortex densities under positive/negative in-plane magnetic fields, respectively.

observed in $Bi_2Te_3/PdTe_2$ heterostructure [25]. At relatively higher temperature, when the B is not completely parallel to the in-plane field, a small B_{OP} component is more likely to induce a vortex which competes with the spontaneous vortex in the BKT phase. Moreover, as shown in Fig. 4(a), a considerable nonreciprocal transport phenomenon ($R^{2\omega}$) can also be observed under zero magnetic field, which may be related to the spontaneous time reversal symmetry broken ferromagnetic layer Ni. To qualitatively study the nonreciprocal transport in Bi/Ni, we calculate the temperature-dependent coefficient γ based on Eq. (3) (see Fig. S4 for details [32]). The temperature dependent γ is summarized in Fig. 4(c) from 2 to 4 K. A kink structure appearing at $T \sim 3$ K indicates that there are two different mechanisms for nonreciprocal transport around the Bi/Ni superconducting transition region which could be separated by mean field temperature (T_{c0}) and BKT temperature (T_{BKT}) at the superconductivity transition region. To extract T_{c0} and T_{BKT}, the temperature-dependent $R^{1\omega}$ at

$B_{IP} = 1.2$ T is fitted based on the Aslamazov-Larkin (AL) [41] and Halperin–Nelson (HN) [42] equations as follows, respectively:

$$R^{1\omega} \propto \left(\frac{1}{R_N} + \alpha\frac{T_{c0}}{T - T_{c0}} + \beta \ln T\right)^{-1}, \quad (4)$$

$$R^{1\omega} \propto R_N \exp\left(-2b\sqrt{\frac{T_{c0} - T}{T - T_{\mathrm{BKT}}}}\right), \quad (5)$$

where α, β, and b are the fitting coefficients. In the AL equation, the first term represents the normal resistance contribution, the second term represents the Cooper pairs fluctuation contribution from thermal excitation when temperature is above T_{c0}, and the third term represents the low temperature $\ln T$ behavior arising from weak (anti)localization and/or electron interaction [43]. In the HN equation, the exponential term describes the spontaneous vortex formation-induced resistance variation due to phase fluctuation as temperature changes from T_{c0} to T_{BKT}. The T_{c0} and T_{BKT} are determined to be 2.89 and 1.72 K, respectively, as shown by the blue and red dashed lines in the inset of Fig. 4(c). Therefore, when $T > 2.89$ K, the nonreciprocal signal can be attributed to the amplitude fluctuation of the superconducting order parameter that gives rise to an additional conductivity [17,21]. For $1.72\ \mathrm{K} < T < 2.89\ \mathrm{K}$, the resistivity state is dominant by the formation of vortex and antivortex at BKT transition due to order parameter phase fluctuation [42]. At the BKT phase transition region, the charge transport is dominated by the spontaneous vortex density and motion which can be modulated by the renormalized current I_r [17,24]. As the B_{IP} direction changes, the renormalized supercurrent I_r is parallel or antiparallel to the applied current I_{sd} which results in the enhancement of channel current to $I_{sd} + I_r$ [Fig. 4(d)] with lower T_{BKT} or suppression of channel current to $I_{sd} - I_r$ [Fig. 4(e)] with higher T_{BKT}, respectively. At the same temperature and amplitude of B_{IP}, the larger channel current of $I_{sd} + I_r$ is more likely to promote vortex formation with higher resistance [Fig. 4(d)] than in the $I_{sd} - I_r$ case [Fig. 4(e)]. Besides, the ability to drive vortex motion varies with different charge current density. Therefore, the magnetic field or I_{sd} direction dependent asymmetric vortex formation and motion result in the nonreciprocal transport behavior at BKT transition region where γ vs T are fitted very well [red line in Fig. 4(c)] based on $\gamma(T) \propto (T - T_{\mathrm{BKT}})^{-1.5}$ as the theoretical expectation of 2D noncentrosymmetric SC [17,21]. As the temperature further decreases to $T = 2$ K, the strong decrease of γ is observed which can be attributed to the freezing vortices at low temperatures.

IV. CONCLUSION

In summary, we report on the nonreciprocal transport in Bi/Ni bilayer, an unconventional p-wave SC candidate. The temperature and magnetic field dependence of the nonreciprocal transport agree well with the theoretical expectation for an in-plane spin-splitting SC. Based on the quantitative analysis of the nonreciprocal transport coefficient, the greatly enhanced nonreciprocal transport in Bi/Ni bilayer can be attributed to the asymmetric vortex motion. Our results, together with previous studies, provide compelling evidence of the Rashba SC in the Bi/Ni bilayer with in-plane spin splitting, a precursor for p-wave SC [6–9], which might hold the promise for future superconducting spintronics and topological quantum computing applications [44].

ACKNOWLEDGMENTS

We acknowledge the financial support from National Basic Research Programs of China (Grants No. 2019YFA0308401, No. 2016YFA0300703, and No. 2022YFA1405100), National Natural Science Foundation of China (Grants No. 11974025, No. 2015CB921402, No. 11374057, No. 11434003, No. 11421404, and No. 12004075), and the Key Research Program of the Chinese Academy of Sciences (Grant No. XDB28000000).

[1] S. Ran, C. Eckberg, Q.-P. Ding, Y. Furukawa, T. Metz, S. R. Saha, I.-L. Liu, M. Zic, H. Kim, J. Paglione *et al.*, Nearly ferromagnetic spin-triplet superconductivity, Science **365**, 684 (2019).

[2] Y. Cao, J. M. Park, K. Watanabe, T. Taniguchi, and P. Jarillo-Herrero, Pauli-limit violation and re-entrant superconductivity in moiré graphene, Nature (London) **595**, 526 (2021).

[3] A. P. Mackenzie and Y. Maeno, The superconductivity of Sr_2RuO_4 and the physics of spin-triplet pairing, Rev. Mod. Phys. **75**, 657 (2003).

[4] D. Aasen, M. Hell, R. V. Mishmash, A. Higginbotham, J. Danon, M. Leijnse, T. S. Jespersen, J. A. Folk, C. M. Marcus, K. Flensberg *et al.*, Milestones Toward Majorana-Based Quantum Computing, Phys. Rev. X **6**, 031016 (2016).

[5] A. Y. Kitaev, Unpaired Majorana fermions in quantum wires, Sov. Phys. Usp. **44**, 131 (2001).

[6] S.-P. Chao, Superconductivity in a Bi/Ni bilayer, Phys. Rev. B **99**, 064504 (2019).

[7] X.-X. Gong, H.-X. Zhou, P.-C. Xu, D. Yue, K. Zhu, X.-F. Jin, H. Tian, G.-J. Zhao, and T.-Y. Chen, Possible p-wave superconductivity in epitaxial Bi/Ni bilayers, Chin. Phys. Lett. **32**, 067402 (2015).

[8] J. Wang, X. Gong, G. Yang, Z. Lyu, Y. Pang, G. Liu, Z. Ji, J. Fan, X. Jing, C. Yang *et al.*, Anomalous magnetic moments as evidence of chiral superconductivity in a Bi/Ni bilayer, Phys. Rev. B **96**, 054519 (2017).

[9] P. Chauhan, F. Mahmood, D. Yue, P. C. Xu, X. Jin, and N. P. Armitage, Nodeless Bulk Superconductivity in the Time-Reversal Symmetry Breaking Bi/Ni Bilayer System, Phys. Rev. Lett. **122**, 017002 (2019).

[10] X. Gong, M. Kargarian, A. Stern, D. Yue, H. Zhou, X. Jin, V. M. Galitski, V. M. Yakovenko, and J. Xia, Time-reversal symmetry-breaking superconductivity in epitaxial bismuth/nickel bilayers, Sci. Adv. **3**, e1602579 (2017).

[11] L. Y. Liu, Y. T. Xing, I. L. C. Merino, H. Micklitz, D. F. Franceschini, E. Baggio-Saitovitch, D. C. Bell, and I. G. Solorzano, Superconductivity in Bi/Ni bilayer system: Clear

role of superconducting phases found at Bi/Ni interface, Phys. Rev. Mater. **2**, 014601 (2018).

[12] V. Siva, K. Senapati, B. Satpati, S. Prusty, D. K. Avasthi, D. Kanjilal, and P. K. Sahoo, Spontaneous formation of superconducting NiBi3 phase in Ni-Bi bilayer films, J. Appl. Phys. **117**, 083902 (2015).

[13] Y. Tokura and N. Nagaosa, Nonreciprocal responses from non-centrosymmetric quantum materials, Nat. Commun. **9**, 3740 (2018).

[14] T. Ideue, K. Hamamoto, S. Koshikawa, M. Ezawa, S. Shimizu, Y. Kaneko, Y. Tokura, N. Nagaosa, and Y. Iwasa, Bulk rectification effect in a polar semiconductor, Nat. Phys. **13**, 578 (2017).

[15] P. He, S. S. L. Zhang, D. Zhu, Y. Liu, Y. Wang, J. Yu, G. Vignale, and H. Yang, Bilinear magnetoelectric resistance as a probe of three-dimensional spin texture in topological surface states, Nat. Phys. **14**, 495 (2018).

[16] R. Aoki, Y. Kousaka, and Y. Togawa, Anomalous Nonreciprocal Electrical Transport on Chiral Magnetic Order, Phys. Rev. Lett. **122**, 057206 (2019).

[17] S. Hoshino, R. Wakatsuki, K. Hamamoto, and N. Nagaosa, Nonreciprocal charge transport in two-dimensional noncentrosymmetric superconductors, Phys. Rev. B **98**, 054510 (2018).

[18] R. Wakatsuki and N. Nagaosa, Nonreciprocal Current in Noncentrosymmetric Rashba Superconductors, Phys. Rev. Lett. **121**, 026601 (2018).

[19] R. Wakatsuki, Y. Saito, S. Hoshino, Y. M. Itahashi, T. Ideue, M. Ezawa, Y. Iwasa, and N. Nagaosa, Nonreciprocal charge transport in noncentrosymmetric superconductors, Sci. Adv. **3**, e1602390 (2017).

[20] E. Zhang, X. Xu, Y.-C. Zou, L. Ai, X. Dong, C. Huang, P. Leng, S. Liu, Y. Zhang, Z. Jia *et al.*, Nonreciprocal superconducting $NbSe_2$ antenna, Nat. Commun. **11**, 5634 (2020).

[21] Y. M. Itahashi, T. Ideue, Y. Saito, S. Shimizu, T. Ouchi, T. Nojima, and Y. Iwasa, Nonreciprocal transport in gate-induced polar superconductor $SrTiO_3$, Sci. Adv. **6**, eaay9120 (2020).

[22] C. Guo, C. Putzke, S. Konyzheva, X. Huang, M. Gutierrez-Amigo, I. Errea, D. Chen, M. G. Vergniory, C. Felser, M. H. Fischer *et al.*, Switchable chiral transport in charge-ordered kagome metal CsV_3Sb_5, Nature (London) **611**, 461 (2022).

[23] Y. Wu, Q. Wang, X. Zhou, J. Wang, P. Dong, J. He, Y. Ding, B. Teng, Y. Zhang, Y. Li *et al.*, Nonreciprocal charge transport in topological kagome superconductor CsV_3Sb_5, npj Quantum Mater. **7**, 105 (2022).

[24] K. Yasuda, H. Yasuda, T. Liang, R. Yoshimi, A. Tsukazaki, K. S. Takahashi, N. Nagaosa, M. Kawasaki, and Y. Tokura, Nonreciprocal charge transport at topological insulator/superconductor interface, Nat. Commun. **10**, 2734 (2019).

[25] M. Masuko, M. Kawamura, R. Yoshimi, M. Hirayama, Y. Ikeda, R. Watanabe, J. J. He, D. Maryenko, A. Tsukazaki, K. S. Takahashi *et al.*, Nonreciprocal charge transport in topological superconductor candidate $Bi_2Te_3/PdTe_2$ heterostructure, npj Quantum Mater. **7**, 104 (2022).

[26] J. Lustikova, Y. Shiomi, N. Yokoi, N. Kabeya, N. Kimura, K. Ienaga, S. Kaneko, S. Okuma, S. Takahashi, and E. Saitoh, Vortex rectenna powered by environmental fluctuations, Nat. Commun. **9**, 4922 (2018).

[27] F. Ando, Y. Miyasaka, T. Li, J. Ishizuka, T. Arakawa, Y. Shiota, T. Moriyama, Y. Yanase, and T. Ono, Observation of superconducting diode effect, Nature (London) **584**, 373 (2020).

[28] H. Narita, J. Ishizuka, R. Kawarazaki, D. Kan, Y. Shiota, T. Moriyama, Y. Shimakawa, A. V. Ognev, A. S. Samardak, Y. Yanase *et al.*, Field-free superconducting diode effect in noncentrosymmetric superconductor/ferromagnet multilayers, Nat. Nanotechnol. **17**, 823 (2022).

[29] C. Baumgartner, L. Fuchs, A. Costa, S. Reinhardt, S. Gronin, G. C. Gardner, T. Lindemann, M. J. Manfra, P. E. Faria Junior, D. Kochan *et al.*, Supercurrent rectification and magnetochiral effects in symmetric Josephson junctions, Nat. Nanotechnol. **17**, 39 (2022).

[30] H. Wu, Y. Wang, Y. Xu, P. K. Sivakumar, C. Pasco, U. Filippozzi, S. S. P. Parkin, Y.-J. Zeng, T. McQueen, and M. N. Ali, The field-free Josephson diode in a van der Waals heterostructure, Nature (London) **604**, 653 (2022).

[31] K. Jiang and J. Hu, Superconducting diode effects, Nat. Phys. **18**, 1145 (2022).

[32] See Supplemental Material at http://link.aps.org/supplemental/10.1103/PhysRevB.108.064501 for the temperature dependent in-plane critical magnetic field; DC measurement of IV characteristics; channel resistance phase diagram as a function of magnetic field and temperature; and detailed parameter extraction process for calculating nonreciprocal coefficients.

[33] J. I. Pascual, G. Bihlmayer, Y. M. Koroteev, H. P. Rust, G. Ceballos, M. Hansmann, K. Horn, E. V. Chulkov, S. Blügel, P. M. Echenique *et al.*, Role of Spin in Quasiparticle Interference, Phys. Rev. Lett. **93**, 196802 (2004).

[34] S. Agergaard, C. Sndergaard, H. Li, M. B. Nielsen, S. V. Hoffmann, Z. Li, and P. Hofmann, The effect of reduced dimensionality on a semimetal: The electronic structure of the Bi(110) surface, New J. Phys. **3**, 15 (2001).

[35] L. P. Gor'kov and E. I. Rashba, Superconducting 2d System with Lifted Spin Degeneracy: Mixed Singlet-Triplet State, Phys. Rev. Lett. **87**, 037004 (2001).

[36] R. Cai, Y. Yao, P. Lv, Y. Ma, W. Xing, B. Li, Y. Ji, H. Zhou, C. Shen, S. Jia *et al.*, Evidence for anisotropic spin-triplet Andreev reflection at the 2D van der Waals ferromagnet/superconductor interface, Nat. Commun. **12**, 6725 (2021).

[37] R. M. Lutchyn, J. D. Sau, and S. Das Sarma, Majorana Fermions and a Topological Phase Transition in Semiconductor-Superconductor Heterostructures, Phys. Rev. Lett. **105**, 077001 (2010).

[38] A. Das, Y. Ronen, Y. Most, Y. Oreg, M. Heiblum, and H. Shtrikman, Zero-bias peaks and splitting in an Al–InAs nanowire topological superconductor as a signature of Majorana fermions, Nat. Phys. **8**, 887 (2012).

[39] A. Sundaresh, J. I. Väyrynen, Y. Lyanda-Geller, and L. P. Rokhinson, Diamagnetic mechanism of critical current nonreciprocity in multilayered superconductors, Nat. Commun. **14**, 1628 (2023).

[40] Y. Hou, F. Nichele, H. Chi, A. Lodesani, Y. Wu, M. F. Ritter, D. Z. Haxell, M. Davydova, S. Ilić, O. Glezakou-Elbert *et al.*, Ubiquitous Superconducting Diode Effect in Superconductor Thin Films, Phys. Rev. Lett. **131**, 027001 (2023).

[41] A. Larkin and A. Varlamov, *Theory of Fluctuations in Superconductors* (Oxford University Press, New York, 2005).

[42] B. I. Halperin and D. R. Nelson, Resistive transition in superconducting films, J. Low Temp. Phys. **36**, 599 (1979).

[43] S. Ichinokura, L. V. Bondarenko, A. Y. Tupchaya, D. V. Gruznev, A. V. Zotov, A. A. Saranin, and S. Hasegawa, Superconductivity in thallium double atomic layer and transition into an insulating phase intermediated by a quantum metal state, 2D Mater. **4**, 025020 (2017).

[44] R. Cai, I. Žutić, and W. Han, Superconductor/ferromagnet heterostructures: A platform for superconducting spintronics and quantum computation, Adv. Quantum Technol. **6**, 2200080 (2022).